Advanced Ceramics Progress: Vol. 7, No. 3, (Summer 2021) 1-9

Materials and Energy Research Center
MERC

Contents lists available at ACERP

Advanced Ceramics Progress

Journal Homepage: www.acerp.ir

Original Research Article

Mechnical Properties and Biocompatibility of Hydroxyapatite/Manganese Dioxide/Palladium Nanocomposite Scaffolds Filled by Natural Chitosan

F. Azizi [a], F. Heidari [b,*], M. Ghaedi [c]

[a] *MS Student, Department of Materials Engineering, Faculty of Engineering, Yasouj University, Yasouj, Kohgiluyeh and Boyer-Ahmad, Iran*
[b] *Assistant Professor, Department of Materials Engineering, Faculty of Engineering, Yasouj University, Yasouj, Kohgiluyeh and Boyer-Ahmad, Iran*
[c] *Professor, Chemistry Department, Yasouj University, Yasouj, Kohgiluyeh and Boyer-Ahmad, Iran*

* Corresponding Author Email: F.heidari@yu.ac.ir (F. Heidari)

URL: https://www.acerp.ir/article_136416.html

ARTICLE INFO

Article History:

Received 18 June 2021
Received in revised form 23 July 2021
Accepted 05 September 2021

Keywords:

Nanocomposite
Cold Isostatic Pressing
Mechanical Properties
Biocompatibility

ABSTRACT

The main objective of the present study is to evaluate the mechanical properties, biocompatibility, and bioactivity behavior of scaffolds made of hydroxyapatite (HA)-modified by MnO_2 and Palladium (Pd) for biomedical applications. Throughout the research, HA, MnO_2, and Pd were developed using sol-gel and precipitation methods, respectively. The properties of the scaffolds were determined using Scanning Electron Microscopy (SEM), Energy Dispersive Spectroscopy (EDX), atomic absorption, and Brunauer−EmmeS−Teller (BET) method. To investigate the in vitro cell proliferation and alkaline phosphatase (ALP) assays, cell culture was done. Furthermore, the mechanical properties of the scaffolds were investigated before and after immersion in Simulated Body Fluid (SBF), and the interaction of Dental Pulp Stem Cells (DPSCs) with the nanocomposite scaffolds was assessed. The obtained results showed that the HA/MnO_2/Pd scaffolds were characterized by higher compressive strength (35.72%), toughness (35.68%), microhardness (80%), and density (0.44%) than HA/MnO_2/Pd filled by chitosan (CS) binder scaffolds. The biocompatibility properties indicated higher cell proliferation and ALP assay on the HA/MnO_2/Pd filled by CS scaffolds than those of HA/MnO_2/Pd scaffolds.

https://doi.org/10.30501/ACP.2021.290650.1067

1. INTRODUCTION

Bone tissue engineering uses both body's natural biological responses to tissue damage and engineering principles as a secondary regeneration strategy for repairing serious bone damages caused by different factors [1,2]. Among the mineral tissues that are extremely efficient in the field of biomedicine are enamel, dentin, and bone [3]. Bone has a high density with a variety of biological, mechanical, and chemical functions [4-6]. Natural bone is a composite of mineral hydroxyapatite (HA) particles reinforced by organic collagen fibers. In addition, HA is the most common bioactive synthetic calcium phosphate ceramic used for bone replacement mainly due to the chemical similarity of its crystal structure with the mineral components of bones and teeth [7,8].

However, due to low fracture toughness and inflexibility, application of HA is mechanically difficult. The inherent fragility of bioceramics overtime limits their clinical applications in biomedicine because their performance is relatively strong when exposed to high

Please cite this article as: Azizi, F., Heidari, F., Ghaedi, M., "Mechnical Properties and Biocompatibility of Hydroxyapatite/Manganese Dioxide/Palladium Nanocomposite Scaffolds Filled by Natural Chitosan", ***Advanced Ceramics Progress***, Vol. 7, No. 3, (2021), 1-9. https://doi.org/10.30501/ACP.2021.290650.1067

pressure, yet quite weak under tensile and shear forces. High compressive strength of ceramics can improve the mechanical properties of the obtained ceramic composites under pressure [9]. Consequently, the reinforced phase in small amounts is a good strategy for enhancing the mechanical and biological properties of HA. So far, HA-based composites have been fabricated by materials such as aluminum oxide, titanium dioxide, carbon, graphene nanotubes, metal fibers, zirconia, and silicon nitride [7].

The molar ratio of Ca/P of apatite is less or more than 1.67 (stoichiometric value for pure HA) depending on the age and type of bone in natural apatite as well as the synthesis method and sintering temperature in artificial apatite. In case the Ca/P ratio is less than 1.67, beta-tricalcium phosphate (β-TCP) and other phases such as tetra-tricalcium phosphate (TTCP) are present in the HA phase. Abnormal phases may adversely affect the biological responses of implants. Moreover, TCP is a biodegradable bioceramic with the chemical formula of $Ca_3(PO_4)_2$. Dissolved in a humid environment, this phase can be replaced by bone during implantation. TCP has four polymorphs, the most common of which are alpha and beta forms [8,10].

Biphasic Calcium Phosphate (BCP) ceramics are a mixture of two phases of HA and β-TCP commonly used in bone repair. It enjoys an advantage, i.e., its chemical properties will alter by changing the HA-to-β-TCP ratio. Higher levels of TCP in BCP cause a higher dissolution rate [11].

Although synthetic HA binds well to the osteoblast cells in body, the rate of differentiation of bone cells is low. HA is excellently bound to the living bone that can stimulate the differentiation of bone cells, and it must be produced with a structure close to that of the mineral phase of a living bone. The mineral phase of a living bone tissue is composed of many ions including fluorine, carbonate, magnesium, manganese, sodium, etc. [12].

The mineral part of the bone with the stoichiometric formula of $Y_2(XO_4)_6Me_{10}$ is known as HA. Bivalent metal cations (Me), anionic trivalent groups (XO_n), and monovalent anion (Y) can easily replace the stoichiometric crystal structure of apatite. Bivalent cations such as Mn^{+2} play an important role in bone metabolism by proliferating osteoblasts and osteoclasts during tissue regeneration. Therefore, as the beneficial effects of Mn^{+2} on HA devices resulting from the applied constraints, the instability of the doped HA structure at high temperatures should be significantly reduced [13,14].

According to the biological studies, manganese is essential for normal bone formation, enzyme function, and amino acid metabolism [15]. Any body without manganese will suffer from several problems such as joint wear, osteoporosis, skeletal deformity, weakness of tendons, and so on. In laboratory animals, the consequences of manganese deficiency are bone deformity, poor growth, impaired reproduction, and blood clotting. Exposure to manganese has been reported to have adverse effects on Central Nervous System (CNS) function and mood. Manganese absorption is inhibited in the presence of excessive amounts of calcium and phosphorus in the diet [16].

Manganese is not found in pure form in nature, and it is mostly present in the form of oxides, carbonates, and silicates. Manganese dioxide (MnO_2), an important adsorbent with a relatively high level, is a microporous structure [17].

In this study, oxidized manganese (MnO_2) was utilized to make a composite and achieve a structure similar to that of the bone mineral phase. One of the reasons for choosing MnO_2 is its effect on fastening the bone growth as well as its biocompatibility and bioactivity [18].

Metal nanoparticles in ceramic scaffolds have several intrinsic properties including antimicrobial activity, mechanical strength, and ability to stimulate osteogenic activity, and angiogenesis in some cases. In addition, metal nanoparticles enjoy the advantage of being safer, more stable, and more likely to stimulate a strong immune response than other materials. Among metal nanoparticles, palladium nanoparticles have recently received considerable attention owing to their prominent catalytic, electronic, magnetic, and optical properties and their particle size and shape [18,19].

Palladium (Pd) has good biocompatibility, which is considered a reasonable choice to maintain the non-toxic properties of nanomaterial; it also has a great potential in biomedicine. For instance, is it commonly used in dental materials and surgical instruments [20,21].

Noble Pd nanoparticles with excellent physicochemical properties such as high thermal stability and good chemical stability can be synthesized in a wide range of sizes and shapes. The overlap of palladium nanoparticles with other biopolymers or molecules results in biocompatible nanoparticles with desirable properties. However, very few studies have employed the unique properties of palladium nanoparticles for textile engineering applications compared to other metals such as gold, silver, or iron. In this regard, this study aims to highlight the potential applications of palladium-based scaffolds in the field of biomedicine [22].

Using reinforced phases such as metal, ceramic, and polymer particles is one of the studied strategies for improving the mechanical properties of apatite implants. Among them, manganese dioxide can improve the mechanical properties of hydroxyapatite due to its desirable properties such as the ability to grow bone, reduce the sintering temperature, and increase the density of HA [23,24].

In our previous research, only the effect of MnO_2 on HA [18] was investigated. The effect of Pd and ZnO on HA [25] was also investigated. In the present study, the simultaneous effect of two MnO_2 and Pd modifiers on HA and the effect of porosity on biocompatibility

behavior and mechanical properties were evaluated. The novelty of this study lies in the fact that the subjects under study have not been published in any other paper.

To be specific, the characterization, microstructure, mechanical and porosity properties, and bioactivity of scaffolds were then investigated. There were two types of scaffolds: HA/MnO_2/Pd and HA/MnO_2/Pd filled by natural chitosan (CS) binder scaffolds (porpos scaffolds) which were compared to each other. To evaluate the biocompatibility scaffold, cell culture was performed with Dental Pulp Stem Cells (DPSCs).

2. MATERIALS AND METHODS

2.1. Praparation of Nano Hydroxyapatite (HA)

Nano-HA was synthesized by the sol-gel method, as previously described [26]. In this way, $Ca(NO_3)_2.4H_2O$ (0.1 M, Sigma-Aldrich, UK), and $(NH_4)_2HPO_4$ (0.06 M, Sigma-Aldrich, UK) were dissolved in deionized water separately, and the pH of both solutions increased up to 11.0 upon the addition of ammonia solution. The solution of $Ca(NO_3)_2.4H_2O$ was added dropwise into the $(NH_4)_2HPO_4$ solution for one h, and the white suspension and gelatinous precipitate were produced. After aging for 24 h at room temperature, the sediments were filtered, washed several times by distilled water, dried at 80 °C, and calcined at 800 °C for one h.

2.2. Preparation of HA/MnO_2/Pd and HA/MnO_2/Pd Filled by Chitosan (CS) Scaffolds

Palladium nitrate (Sigma-Aldrich, UK) and $KMnO_4$ (Sigma-Aldrich, UK) solutions were mixed at room temperature. Nano-HA was then added to this solution. The mixture was stirred for three hours at 70 °C. The precipitate was then centrifuged, filtered, and washed with water several times; then, it was dried at 80 °C. The precipitates were calcined at 450 °C for two hours. The prepared powder was added to the 2% (v/v) acetic acid solution. The suspension was stirred for one h at 50 °C. Then, 0.15 g chitosan (CS) (Sigma-Aldrich, UK) was added into the solution and stirred for 1 h to prepare a gelous suspension. This gel was dried at 60 °C for 24 h and then, it was milled.

The prepared powders, coated by CS and non-coated by CS, were pressed using the Cold Isostatic Pressing (CIP) technique at 250 MPa to prepare circular discs. Samples of 10 mm in diameter and 4mm in height were prepared for microhardness test, density measurement, and cell culture, respectively. To perform the compression test, the samples were made in the shape of a cylinder with the diameter and height of 10 mm. The sintering temperature was at 1450 °C for two hours with the heating rate of 5 °C/min. In this study, HA/MnO_2/Pd and HA/MnO_2/Pd filled by CS (0.15 g) were prepared, respectively [25].

2.3. Material Characterization

To determine HA, MnO_2, and Pd contents within the HA/MnO_2/Pd and HA/MnO_2/Pd filled by CS scaffolds, an AA680 atomic absorption/flame mission spectrophotometer (Shimadzu, Japan) was utilized. A SEM equipped with Energy Dispersive Spectroscopy (EDS) was employed to examine the morphology of scaffolds. The porosity of scaffolds was also investigated using SEM. A transmission electron microscope (TEM; JEOL JEM-2100, Japan) was employed to investigate the morphology and determine the size of the nanoparticles in the composites powder.

The porosity properties of samples were estimated by Brunauer−EmmeS−Teller (BET) method to determine the specific surface area.

2.4. Evaluation of Mechanical Properties

Compressive and hardness tests were carried out to evaluate the mechanical properties. The compressive strength test was performed using a universal testing machine (Zwick, Material Prufung, 1446e60) with a load cell of 10 kN. The crosshead speed of compressive mechine was 0.5 mm/min [27]. The toughness of the samples was calculated by surface area calculation of stress-strain curve. The microhardness (Hv) of the polished sintered disc shape samples was determined by the Vickers indentation (MHV1000Z) and an applied load of 200 g with a dwell time of 10 s. The density was measured by the Archimedes method.

2.5. Bioactivity, Cell Culture, and ALP Assay

The sintered HA samples were immersed in 20 mL of Simulated Body Fluid (SBF) [28]. The samples were kept in Ben Marie bath at 37 °C for 28 days and were dried at room temperature. Changes in the surface morphologies of samples before and after soaking in the SBF were investigated using SEM and EDX.

To sterilize the samples for cell culture, they were washed in 70% ethanol three times and then, they washed with Phosphate Buffer Saline (PBS) for 15 min/cycle. Culture medium was prepared from Dulbecco's Modified Eagle Medium (DMEM, Sigma, USA) supplemented with 10% fetal bovine serum (FBS, Sigma, USA) and 1% Penicillin-Streptomycin (Invitrogen, USA). Human osteoblast cells (HOB, Cell Applications, USA) with the dimentions of 5×10^5 were cultured on the samples immersed in a culture medium. The medium was refreshed every two days.

Dental pulp stem cells were also used for cell culture. After defrosting the cells, they were transformed to a flask containing RPMI culture medium containing 10% FBS and then, the flask was placed in an incubator at 37 °C. The cells were then cultured in a culture medium containing scaffolds for seven days and finally, the microstructure of the cells was examined using the fluorescence microscope.

In order to measure the activity of alkaline phosphate, first, 10 thousand HOB cells were poured on each of the scaffolds and 100 µl of culture medium was added to each scaddold; after three hours, one ml of culture medium was added to facilitate the addition of the cells to the scaffold. After 24 hours, one ml of culture medium was added to the samples and after 14 days, the culture medium was collected on the samples and cell lysates were recognized for protein content using a micro-BCA assay kit (Pierce) and ALP was normalized to the total protein content, measured using Pierce BCA protein assay kit. Triplicate samples were used for this ALP experiment. All data were shown as the mean ± standard deviation (Mean ± SD). The significant difference was analyzed by ANOVA complemented by Tukey's multiple comparisons test. P-values < 0.05 were considered as statistically significant.

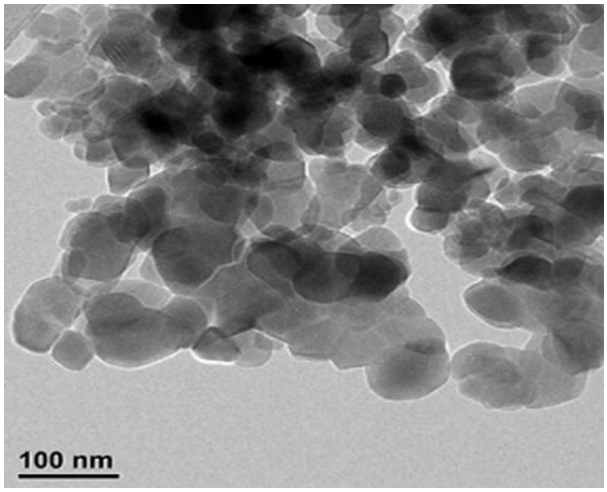

Figure 1. TEM image of HA/MnO_2/Pd powders

3. RESULTS AND DISCUSSION

3.1. Atomic Absorption Analysis and Microstructure of HA/MnO_2/Pd Powder

Atomic absorption analysis was conducted on HA/MnO_2/Pd composite powder. Here, 0.02 g of this composite powder was used and dissolved in 28 cc solvent (chloridric acid) and the concentrations of Mn^{2+}, Ca^{2+}, and Pd^{2+} ions were to be 0.46, 211, and 0.67 mg/l, respectively.

The ion contents in nanocomposite include 5.86, 0.015, and 0.021 mg of calcium, manganese, and palladium ions, respectlively, in a liter of solvent. Given that the selection of 0.02 g of powder for atomic absorption was used, the total amount of Mn^{2+}, Ca^{2+}, and Pd^{2+} ions in the total powder was 0.07, 29.17, and 0.098%, respectively. The molecular weights of Mn, Ca, and Pd were 54.94, 40, and 106.42 g/mol, resepctively, and the molecular weight of oxygen was 16 g/mol. Therefore, MnO_2 deposited on HA is equal to 70.94 ×0.07%, which is approximately 0.05%; however, Pd deposited on HA/MnO_2 is equal to 106.42×0.098%, which is approximately 0.104%. Due to the molecular weight of $KMnO_4$ solution and $Pd(NO_3)_2$, $2H_2O$ and an initial amount of palladium salt, potassium permanganate salt, and HA were utilized in this study. Mn^{2+} and Pd^{2+} contributions are 11.8% and 2.13%, which, in proportion to the initial HA weight used (2 g), should be in the composite 4.6% and 0.82%. This is the reason why X-ray diffraction could not show MnO_2 and Pd peaks; therefore, these two phases were characterized by atomic absorption and EDS.

Figure 1 indicates TEM image of HA/MnO_2/Pd powder. All of the particles shown in this figure are less than 100 nm. Therefore, HA, MnO_2 and Pd are measured on a nano-scale scale.

3.2. Scanning Electron Microscope Images Before and After Immersion in SBF and Porosity Properties

Figures. 2(a) and (b) illustrate the cross-section of HA/MnO_2/Pd scaffolds before immersion in SBF. Figure 2a shows the cross-sectional area of HA/MnO_2/Pd sintered scaffold at 1400 °C and the effect of Pd on the HA/MnO_2 composite. As shown in Figure. 2(a), addition of Pd leads to a dense structure, and the porosity in these scaffolds is lower than that in Figure 2(c) which shows HA/MnO_2/Pd filled by CS scaffold. Figure 2(c) shows the spherical porosity in the scaffold matrix after coating HA/MnO_2 with CS. Increasing porosity can affect the mechanical properties and biocompatiblities of the scaffolds. In this respect, these properties are fully discussed in the following sections. Figure 2(d) shows the EDX analysis of the HA/MnO_2/Pd filled by CS scaffold which confirms the presence of Mn and Pd in the composite.

SEM images (Figure 3a and b) show the sediments on the surface of the HA/MnO_2/Pd and HA/MnO_2/Pd filled by CS. Both of sedimentations are perfectly uniform. The EDS pattern of the apatite formed on the surface of the HA/MnO_2/Pd sample after immersion in the SBF is illustrated in Figure 3c. In this pattern (Figure 3c), the characteristic peak of the apatite containing Ca, P, and O has high intensity. In fact, upon immersing in the SBF, the ions in the SBF solution were sedimented on the scaffold surface. Table 1 presents the quantitative results of EDX analysis from apatite precipitation on samples after 28 days of immersion in SBF. The ratio of Ca/P is 1.66, confirming the formation of apatite on the surface.

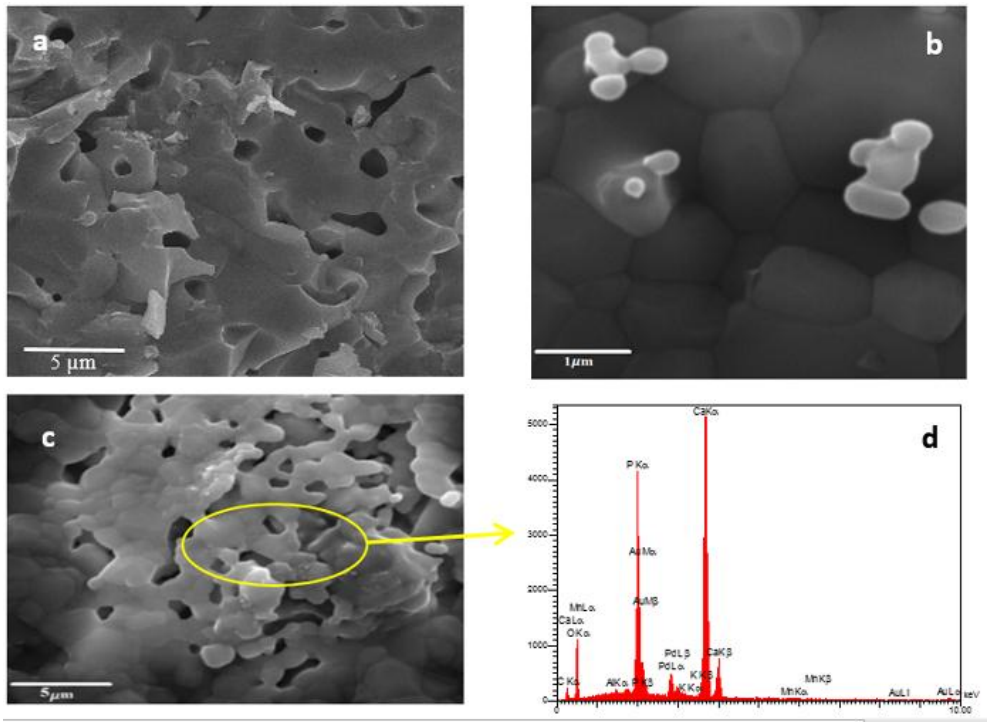

Figure 2. SEM images of (a,b) the cross-sectional area at the fracture of the HA/MnO_2/Pd at two magnifications before immersion in SBF, (c) the cross-sectional area at the fracture of the HA/MnO_2/Pd filled by CS before immersion in SBF, and (d) EDX analysis from HA/MnO_2/Pd filled by CS

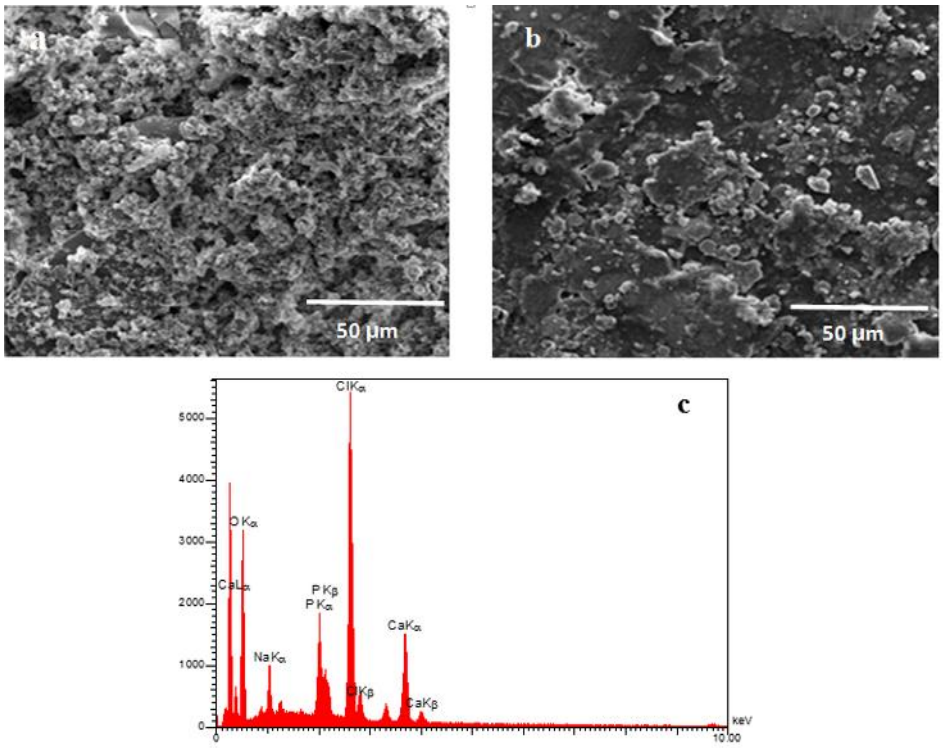

Figure 3. The morphology of apatite crystals formed on the surface of samples after 28 days of immersion in SBF: (a) HA/MnO_2/Pd, (b) HA/MnO_2/Pd filled by CS, and (c) EDX analysis of the apatite formed on the surface of the HA/MnO_2/Pd sample after immersion in the SBF

TABLE 1. Quantitative results of EDX analysis from apatite precipitation on samples after 28 days of immersion in SBF

Elem.	Line	Int.	Err.	K	K_r	wt%	at.%	ZAF
O	Ka	269.9	238.1921	0.366	0.159	61.44	77.47	0.2537
Na	Ka	84.4	27.0804	0.037	0.016	5.36	4.61	0.3056
P	Ka	278.4	100.0868	0.119	0.052	6.33	4.32	0.7675
Cl	Ka	601.7	4.2802	0.305	0.133	16.34	9.12	0.8134
Ca	Ka	268.2	2.2779	0.169	0.073	10.53	4.48	0.8516
				1.000	0.434	100.0	100.0	

The reasons behind the formation of porosities in scaffolds were the incorporation of the CS binder and its removal. Table 2 shows the the porosity in these scaffolds, the porosity parameters of HA/MnO_2/Pd, and HA/MnO_2/Pd filled by CS scaffolds. The HA/MnO_2/Pd filled by the CS sample has a higher specific surface area than the HA/MnO_2/Pd samples. The specific surface area of the HA/MnO_2/Pd filled by CS sample is 2.5 units higher than that of HA/MnO_2/Pd samples, respectively. Further, the total pore volume and mean pore diameter parameters of the HA/MnO_2/Pd filled by CS sample are more than those of the HA/MnO_2/Pd samples.

TABLE 2. Porosity parameters of HA/MnO_2/Pd and HA/MnO_2/Pd filled by CS samples

Parameter	HA/MnO_2/Pd	HA/MnO_2/Pd filled by CS
BET specific surface area (m^2 g^{-1})	3.3963	8.6547
Total pore volume (cm^3 g^{-1})	0.0101	0.01912
Mean pore diameter (nm)	1.0102	12.654

3.3. Density and Mechanical Testing

According to Table 3, the bulk density of the HA/MnO_2/Pd is more than HA/MnO_2/Pd filled by CS scaffolds. This difference depends on the number of porosities in the scaffolds. The amount of porosities also depends on the amount of CS filled on the surface of the HA/MnO_2/Pd powder.

The hardness of the samples is given in Table 2. The results revealed that the hardness of the HA/MnO_2/Pd sample was more than that of HA/MnO_2/Pd filled by CS scaffolds. Given that the density of this sample is lower, it has more porosity and, hence, less hardness.

TABLE 3. Bulk density and hardness of HA/MnO_2/Pd and HA/MnO_2/Pd filled by CS

Composition	Density (g/cm^3)	Hardness (GPa)
HA-MnO_2-Pd	2/4119	1.05
HA-MnO_2-Pd-filled by Cs	2/4012	0.21

Figure 4 and Table 4 indicate the compressive strength of the samples. Sample HA/MnO_2/Pd has higher compressive strength than that of sample HA/MnO_2/Pd filled by CS. This increase in the compressive strength can be attributed to the higher density of this sample (Table 3). There is also this process after immersion. However, the difference in the compressive strength before and after immersion in HA/MnO_2/Pd sample is greater than that in HA/MnO_2/Pd filled by CS, indicating that the compressive strength would decreased significantly due to the presence of porosities in the sample and absorption of solution into the open porositeis. Moreover, a comparison of this study with that conducted by Azizi et al. revealed that after immersion in SBF solution, the mechanical properties of both of HA/MnO_2/Pd and HA/MnO_2/Pd filled by CS scaffolds were higher than those of pure HA before immersion, mainly due to the cohesiveness of the ceramic matrix (HA/MnO_2) in the presence of Pd metal nanoparticles. Thereofore, it can be concluded that incorporation of palladium to HA and HA/MnO_2 would increase the hardness, toughness, and compressive strength [18].

TABLE 4. Compressive strength and toughness of HA/MnO_2/Pd and HA/MnO_2/Pd filled by CS before and after immersion in SBF for 28 days

		HA/MnO_2/Pd	**HA/MnO_2/Pd filled by CS**
Compressive Strength (MPa)	Before immersion	167.45	107.64
	After immersion	76.38	54.52
Toughness (MPa)	Before immersion	1.803	1.159
	After immersion	0.823	0.587

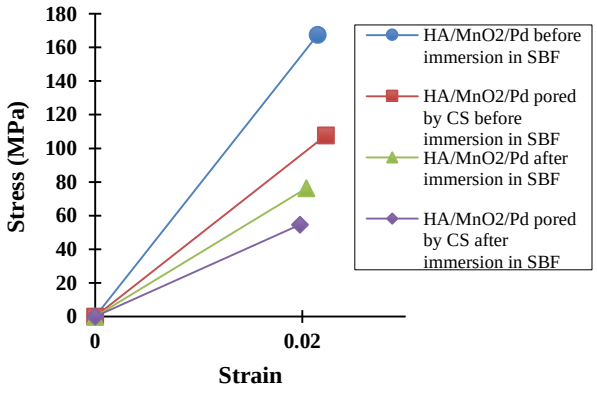

Figure 4. Compressive stress-strain curves of HA/MnO_2/Pd and HA/MnO_2/Pd filled by CS befpre and after immersion in SBF solution

Incorporation of metal nanoparticles improves the mechanical properties of ceramic composites. In general, porosity can reduce the mechanical properties of the HA/MnO_2/Pd filled by CS scaffolds compared to the samples without porosity (HA/MnO_2/Pd); however, compared to the study of Azizi et al., even after 28 days of immersion, the porous scaffolds (HA/MnO_2/Pd filled by CS) outperformed the HA/MnO_2 samples [18]. Chowhury indicated that the compressive strength, hardness, and Young's modulus of ceramic composites decreased upin increasing the porosity [29].

3.4. In Vitro Evaluation

Deposition of Pd and MnO_2 on HA increased its biocompatibility. Azizi et al. previously cultured the same cell on HA produced by sol-gel method and HA/MnO_2 nanocomposite, and they found that MnO_2 caused a slight decrease in the biocompatibility of HA [18]. According to the result of this study, Pd was added to HA/MnO_2 nanocomposites, and the biocompatibility of HA/MnO_2/Pd nanocomposite scaffolds was much higher than that of pure HA and HA/MnO_2 scaffolds. Moreover, increasing the porosity of HA/MnO_2/Pd by CS binder would increase the biocompatibility of this nanocomposite even more. Therefore, it can be concluded that Pd and porosity together are factors that can play a key in increasing cell proliferation.

It is predicted that nano-scale ceramic scaffolds in this study, in addition to the desired mechanical properties, due to the high specific surface area of the particles, also have higher bioactivity than conventional composites based on hydroxyapatite and thus, they can be used as the tissue increases under load. The density, sinterability, and mechanical properties of ceramics made from nanoscale powders can be enhanced using hydroxyapatite nanocrystals, which are acknowledged to be better biocompatible with larger crystals [30].

Previous research has shown that scaffolds with high porosity could exhibit higher surface area, hence higher biodegradability [31]. At the surface roughness more than 50 nm, van der Waals forces are the main factor; however, at less distances between 10–20 nm, a combination of both van der Waals forces and electrostatic interactions affect the cell adhesion [32]. In medical implants made by metals, the desired surface roughness is usually less than 10 nm [33]. Rough surface promotes friction, thus decreaseing the mobility of the bacteria; this sessile environment improves the biofilm growth [34]. Hence, HA/MnO_2/Pd filled by CS scaffolds have a significant surface roughness that can be a good place for cell proliferation. Figure 5(b) shows ALP assay of the HA/MnO_2/Pd and HA/MnO_2/Pd filled by CS scaffolds. The observed trend for the cell proliferation diagram (Figure 5(a)) was also observed in this diagram (Figure 5(b)). A comparison between this study and that of Heidari et al., who assessed the HA/ZnO/Pd nanocomposites, revealed that the sedimentation of Pd and ZnO on HA reduced its biocompatibility. According to the obtained results, it can be concluded that the decrease in the biocompatibility of HA/ZnO/Pd nanocomposite compared to pure HA resulted from Zn ions leakage, and Pd did not play any role in this reduction [25,35-36].

The small particle size of the nanocomposite facilitates its penetration into the bacterial cell membrane and destructs the cell cytoplasm and nucleic acids leading to cell death. The cellular response of toxicant is determined by viability assays. The toxic effect of nanocomposites on biological cells is known as cytotoxicity that depends on different characteristics. In order to prepare the non-toxic composites, more emphsis should be put on the selection of metal to be incorporated. In this respect, optimum incorporation of Pd nano particles to the nanocomposite is essential for better cell viability. Lateral dimensions, amount of oxygen groups, large surface area, and selection of the material for incorporation provide better cell viability of Pd/ZnO that makes the nanocomposite a promising biocompatible and nontoxic nanomaterial used as an apoptosis agent for the appropriate drug delivery system in various biomedical applications [37].

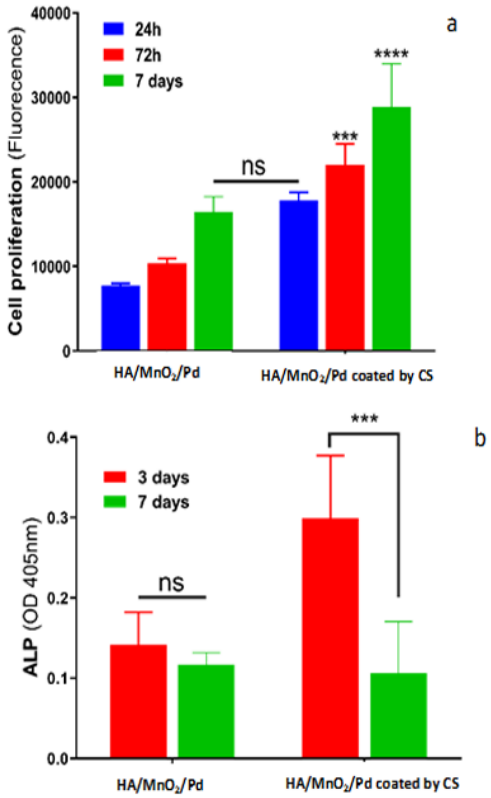

Figure 5. Cell proliferation diagrams on (a) HA/MnO_2/Pd and HA/MnO_2/Pd filled by CS scaffolds, (b) ALP assessment on HA/MnO_2/Pd and HA/MnO_2/Pd filled by CS scaffold after 7 days

4. CONCLUSION

Two types of scaffolds containing HA, MnO_2, and Pd were prepared and characterized in this study. HA/MnO_2/Pd filled by CS had lower mechanical properties than those of HA/MnO_2/Pd scaffolds before and after immersion in SBF solution. The results indicated that HA/MnO_2/Pd nanocomposite scaffold was characterized by better cell viability and biocompatibility than those of HA/MnO_2/Pd scaffolds.

ACKNOWLEDGEMENTS

This study is a part of the research master plan of Fatemeh Heidari supported by Yasouj University. The authors gratefully thank Marquette University for cell culture and ALP assay.

REFERENCES

1. Akbarpoor, S., Karbasi, S., "Evaluation of Physical and Mechanical Properties of Hydroxyapatite/Titanium dioxide Composite Scaffold for Tissue Engineering Applications", ***Journal of Advanced Materials and Technologies***, Vol. 3, No. 3, (2014), 17-26. https://doi.org/10.30501/JAMT.2635.70268
2. Bose, S., Sarkar, N., "Natural medicinal compounds in bone tissue engineering", ***Trends in Biotechnology***, Vol. 38, No. 4, (2020), 404-417. https://doi.org/10.1016/j.tibtech.2019.11.005
3. Lopes, C. D. C. A., Limirio, P. H. J. O., Novais, V. R., Dechichi, P., "Fourier transform infrared spectroscopy (FTIR) application chemical characterization of enamel, dentin and bone", ***Applied Spectroscopy Reviews***, Vol. 53, No. 9, (2018), 747-769. https://doi.org/10.1080/05704928.2018.1431923
4. Rho, J. Y., Kuhn-Spearing, L., Zioupos, P., "Mechanical properties and the hierarchical structure of bone", ***Medical Engineering & Physics***, Vol. 20, No. 2, (1998), 92-102. https://doi.org/10.1016/s1350-4533(98)00007-1
5. Shao, J., Wang, Z., Yang, T., Ying, H., Zhang, Y., Liu, S., "Bone regulates glucose metabolism as an endocrine organ through osteocalcin", ***Internatinal Journal of Endocrinology***, (2015), 1-9. https://doi.org/10.1155/2015/967673
6. Song, L., "Calcium and bone metabolism indices", ***Advanced in Clinical Chemistry***, Vol. 82, (2017), 1-46. https://doi.org/10.1016/bs.acc.2017.06.005
7. Darvishalipour, F., Ghafouri Taleghani, H., Ghorbani, M., Salimi Kenari, H., "Fabrication of nanoporous functionalized hydroxyapatite as high performance adsorbent for Acid Blue 25 dye removal", ***International Journal of Engineering***, Vol. 32, No. 2, (2019), 193-200. https://www.ije.ir/article_82476_09f6d62ffdfc097666a36cad4b2fb65c.pdf
8. LeGeros, R. Z., "Biodegradation and bioresorption of calcium phosphate ceramics", ***Clinical Materials***, Vol. 14, No. 1, (1993), 65-88. https://doi.org/10.1016/0267-6605(93)90049-D
9. Akpan, E. S., Dauda, M., Kuburi, L. S., Obada. D. O., Dodoo-Arhin, D., "A comparative study of the mechanical integrity of natural hydroxyapatite scaffolds prepared from two biogenic sources using a low compaction pressure method", ***Results in Physics***, Vol. 17, (2020), 103051. https://doi.org/10.1016/j.rinp.2020.103051
10. Coelho, W. T., Fernandes, J. M., Escobar, C. F., Thurmer, M. B., Santos, L. A., "Modifications on the properties of a Calcium Phosphate Cement after addition of 1, 2 and 3% Sodium Alginate", In ***56º Congresso Brasileiro de Cerâmica, 1º Congresso Latino-Americano de Cerâmica, IX Brazilian Symposium on Glass and Related Materials***, Curitiba, 3-6 June 2012, Brasil, (2012), 1822-1827. https://abceram.org.br/wp-content/uploads/area_associado/56/PDF/12-015.pdf
11. Zhang, K., Zhang, J., Chen, K., Hu, X., Wang, Y., Yang, X., Zhang, X., Fan, Y., "In vitro and in vivo assessment of nanostructured porous biphasic calcium phosphate ceramics for promoting osteogenesis in an osteoporotic environment", ***RSC Advances***, Vol. 8 No. 26, (2018), 14646-14653. https://doi.org/10.1039/c8ra00768c
12. Khalili, A., Naeimi, F., Fakhrizadeh, A. A., "Electrodeposited Hydroxyapatite/Graphene Oxide/Zirconia Oxide Composite Coatings: Characterization and Antibacterial Activity", ***Advanced Ceramics Progress***, Vol. 6, No. 4, (2020), 8-14. https://doi.org/10.30501/acp.2020.233349.1037
13. Moreira, M. P., de Almeida Soares, G. D., Dentzer, J., Anselme, K., de Sena, L. Á., Kuznetsov, A., dos Santos, E. A., "Synthesis of magnesium-and manganese-doped hydroxyapatite structures assisted by the simultaneous incorporation of strontium", ***Materials Science and Engineering: C***, Vol. 61, (2016), 736-743. https://doi.org/10.1016/j.msec.2016.01.004
14. Slater, N., Dasmah, A., Sennerby, L., Hallman, M., Piattelli, A., Sammons, R., "Back-scattered electron imaging and elemental microanalysis of retrieved bone tissue following maxillary sinus floor augmentation with calcium sulphate", ***Clinical Oral Implants Research***, Vol. 19, No. 8, (2008), 814-822. https://doi.org/10.1111/j.1600-0501.2008.01550.x
15. Scheideler, S. E., "Interaction of dietary calcium, manganese, and manganese source (Mn oxide or Mn methionine complex) on chick performance and manganese utilization", ***Biological Trace Element Research***, Vol. 29, No. 3, (1991), 217-228. https://doi.org/10.1007/BF03032679
16. Soetan, K. O., Olaiya, C. O., Oyewole, O. E., "The importance of mineral elements for humans, domestic animals and plants-A review", ***African Journal of Food Science***, Vol. 4, No. 5, (2010), 200-222. https://doi.org/10.5897/AJFS.9000287
17. Dong, L., Zhu, Z., Qiu, Y., Zhao, J., "Removal of lead from aqueous solution by hydroxyapatite/manganese dioxide composite", ***Frontiers of Environmental Science & Engineering***, Vol. 10, No. 1, (2016), 28-36. https://doi.org/10.1007/s11783-014-0722-5
18. Azizi, F., Heidari, F., Fahimipour, F., Sajjadnejad, M., Vashaee, D., Tayebi, L., "Evaluation of mechanical and biocompatibility properties of hydroxyapatite/manganese dioxide nanocomposite scaffolds for bone tissue engineering application", ***Internatinal Journal of Applied Ceramic Technology***, Vol. 17, No. 5, (2020), 2439-2449. https://doi.org/10.1111/ijac.13549
19. Calabrese, G., Petralia, S., Fabbi, C., Forte, S., Franco, D., Guglielmino, S., Esposito, E., Cuzzocrea, S., Traina, F., Conoci, S., "Au, Pd and maghemite nanofunctionalized hydroxyapatite scaffolds for bone regeneration", ***Regenerative Biomaterials***, Vol. 7, No. 5, (2020), 461-469. https://doi.org/10.1093/rb/rbaa033
20. Zhang, X., Cheng, G., Xing, X., Liu, J., Cheng, Y., Ye, T., Wang, Q., Xiao, X., Li, Z., Deng, H., "Near-infrared light-

triggered porous AuPd alloy nanoparticles to produce mild localized heat to accelerate bone regeneration", ***The Journal of Physical Chemistry Letters***, Vol. 10, No. 15, (2019), 4185-4191. https://doi.org/10.1021/acs.jpclett.9b01735

21. Huang, T., Cheng, J., Zheng, Y. F., "In vitro degradation and biocompatibility of Fe–Pd and Fe–Pt composites fabricated by spark plasma sintering", ***Materials Science and Engineering: C***, Vol. 35, (2014), 43-53. https://doi.org/10.1021/acsbiomaterials.0c00263
22. Phan, T. T. V., Huynh, T. C., Manivasagan, P., Mondal, S., Oh, J., "An up-to-date review on biomedical applications of palladium nanoparticles", ***Nanomaterials***, Vol. 10, No. 1, (2020), 66. https://doi.org/10.3390/nano10010066
23. Kumar, S., Adjei, I. M., Brown, S., Liseth, O., Sharma, B., "Manganese dioxide nanoparticles modulate oxidative stress and protect cartilage from interleukin-1β induced degradation", ***Osteoarthritis and Cartilage***, Vol. 27, (2019), S81-S82. https://doi.org/10.1016/j.joca.2019.02.115
24. Ramesh, S., Tan, C. Y., Peralta, C. L., Teng, W. D., "The effect of manganese oxide on the sinterability of hydroxyapatite", ***Science and Technology of Advanced Materials***, Vol. 8, No. 4, (2007), 257-263. https://doi.org/10.1016/j.stam.2007.02.006
25. Heidari, F., Tabatabaei, F. S., Razavi, M., Lari, R. B., Tavangar, M., Romanos, G. E., Vashaee, D., Tayebi, L., "3D construct of hydroxyapatite/zinc oxide/palladium nanocomposite scaffold for bone tissue engineering", ***Journal of Materials Science: Materials in Medicine***, Vol. 31, No. 10, (2020), 1-14. https://doi.org/10.1007/s10856-020-06409-2
26. Dastoorian, F., Salem, A., Salem, S., "Fabrication of poorly crystalline hydroxyapatite nano-particles by rapid auto-ignition route as efficient adsorbent for removal of disperse blue dye", ***Journal of Alloys and Compounds***, Vol. 766, No. 1, (2018), 729-738. https://doi.org/10.1016/j.jallcom.2018.07.042
27. Heidari, F., Razavi, M., Ghaedi, M., Forooghi, M., Tahriri, M., Tayebi, L., "Investigation of mechanical properties of natural hydroxyapatite samples prepared by cold isostatic pressing method", ***Journal of Alloys and Compounds***, Vol. 693, (2017), 1150-1156. https://doi.org/10.1016/j.jallcom.2016.10.081
28. Mobasherpour, I., Salahi, E., Razavi, M., Asjodi, A., "In vitro evaluation of apatite/wollastonite glass–ceramic nano biocoatings on 316 steel alloys by plasma-sprayed", ***Advanced Ceramics Progress***, Vol. 1, No. 3, (2015), 34-38. https://doi.org/10.30501/ACP.2015.70010
29. Natasha, A. N., Sopyan, I., Zuraida, A., "Fourier transform infrared study on sol-gel derived manganese-doped hydroxyapatite", ***Advanced Materials Research***, Vol. 47-50, (2008), 1185-1188. https://doi.org/10.4028/www.scientific.net/AMR.47-50.1185
30. Chowdhury, A., "Constitutive modelling and Weibull statistical analysis for the porosity-mechanical property correlations in 3% yittria-stabilized zirconia system", ***International Journal of Refractory Metals and Hard Materials***, Vol. 70, (2018), 246-252. https://doi.org/10.1016/j.ijrmhm.2017.10.020
31. Gheysari, H., Mohandes, F., Mazaheri, M., Dolatyar, B., Askari, M., Simchi, A., "Extraction of hydroxyapatite nanostructures from marine wastes for the fabrication of biopolymer-based porous scaffolds", ***Marine Drugs***, Vol. 18, No. 1, (2020), 26. https://doi.org/10.3390/md18010026
32. Savjani, K. T., Gajjar, A. K., Savjani, J. K., "Drug solubility: importance and enhancement techniques", ***International Scholarly Research Notices***, Vol. 2012, (2012), Article ID 195727, 1-10. https://doi.org/10.5402/2012/195727
33. Percival, S. L., Malic, S., Cruz, H., Williams, D. W., "Introduction to biofilms", In Percival S., Knottenbelt D., Cochrane C. (eds.) ***Biofilms and Veterinary Medicine***, Springer Series on Biofilms, vol, 6, Springer, Berlin, Heidelberg, (2011), 41-68. https://doi.org/10.1007/978-3-642-21289-5_2
34. Mendonça, G., Mendonça, D. B., Aragao, F. J., Cooper, L. F., "Advancing dental implant surface technology–from micron-to nanotopography", ***Biomaterials***, Vol. 29, No. 28, (2008), 3822-3835. https://doi.org/10.1016/j.biomaterials.2008.05.012
35. Golabi, M., Turner, A. P., Jager, E. W., "Tunable conjugated polymers for bacterial differentiation", ***Sensors and Actuators B: Chemical***, Vol. 222, (2016), 839-848. https://doi.org/10.1016/j.snb.2015.09.033
36. Tavangar, M., Heidari, F., Hayati, R., Tabatabaei, F., Vashaee, D., Tayebi, L., "Manufacturing and characterization of mechanical, biological and dielectric properties of hydroxyapatite-barium titanate nanocomposite scaffolds", ***Ceramics International***, Vol. 46, No. 7, (2020), 9086-9095. https://doi.org/10.1016/j.ceramint.2019.12.157
37. Rajeswari, R. and Prabu, H. G., "Palladium–Decorated reduced graphene oxide/zinc oxide nanocomposite for enhanced antimicrobial, antioxidant and cytotoxicity activities", ***Process Biochemistry***, Vol. 93, (2020), 36-47. https://doi.org/10.1016/j.procbio.2020.03.010